A&A 477, 641–647 (2008)
DOI: 10.1051/0004-6361:20078488

Astronomy & Astrophysics

Search for vertical stratification of metals in atmospheres of blue horizontal-branch stars⋆

V. R. Khalack[1], F. LeBlanc[1], B. B. Behr[2,⋆⋆], G. A. Wade[3], and D. Bohlender[4]

[1] Département de Physique et d'Astronomie, Université de Moncton, Moncton, N.-B., E1A 3E9, Canada
e-mail: khalakv@umoncton.ca
[2] Department of Astronomy, University of Texas at Austin, 1 University Station C1400, Austin TX 78712-0259, USA
[3] Department of Physics, Royal Military College of Canada, PO Box 17000 stn "FORCES", Kingston, Ontario, K7K 4B4, Canada
[4] National Research Council of Canada, Herzberg Institute of Astrophysics, 5071 West Saanich Road, Victoria, BC, V9E 2E7, Canada

Received 15 August 2007 / Accepted 19 October 2007

ABSTRACT

Context. The observed abundance peculiarities of many chemical species relative to the expected cluster metallicity in blue horizontal-branch (BHB) stars presumably appear as a result of atomic diffusion in the photosphere. The slow rotation (typically $v \sin i < 10$ km s^{-1}) of BHB stars with effective temperatures $T_{\rm eff} > 11\,500$ K supports this idea since the diffusion mechanism is only effective in a stable stellar atmosphere.
Aims. In this work we search for observational evidence of vertical chemical stratification in the atmospheres of six hot BHB stars: B84, B267 and B279 in M 15 and WF2-2541, WF4-3085 and WF4-3485 in M 13.
Methods. We undertake an abundance stratification analysis of the stellar atmospheres of the aforementioned stars, based on acquired Keck HIRES spectra.
Results. We have found from our numerical simulations that three stars (B267, B279 and WF2-2541) show clear signatures of the vertical stratification of iron whose abundance increases toward the lower atmosphere, while the other two stars (B84 and WF4-3485) do not. For WF4-3085 the iron stratification results are inconclusive. B267 also shows a signature of titanium stratification. Our estimates for radial velocity, $v \sin i$ and overall iron, titanium and phosphorus abundances agree with previously published data for these stars after taking the measurement errors into account. The results support the hypothesis regarding the efficiency of atomic diffusion in the stellar atmospheres of BHB stars with $T_{\rm eff} > 11\,500$ K.

Key words. stars: atmospheres – stars: horizontal-branch – stars: chemically peculiar

1. Introduction

According to the current understanding of stellar evolution, the horizontal-branch (HB) stars are post-main sequence stars that burn helium in their core and hydrogen in a shell (e.g. Moehler 2004). In this paper we consider the HB stars that are located in the blue part of the HB, to the left of the RR Lyrae instability strip. Most researchers call them blue horizontal-branch (BHB) stars to distinguish them from the red horizontal-branch (RHB) stars, which exhibit different observational properties. Sandage & Wallerstein (1960) have found from analysis of the colour−magnitude diagrams of globular clusters[1] that the HB generally becomes bluer with decreasing metallicity. Derived masses of the cool ($T_{\rm eff} < 11\,500$ K) BHB stars in the globular cluster NGC 6388 (Moehler & Sweigart 2006) are in a good agreement with the predictions of canonical HB evolution, except for the hot BHB stars with $T_{\rm eff} > 11\,500$ K, where the estimated stellar masses seem to be lower than the canonical values.

The Hertzsprung-Russell diagrams of some globular clusters show long blue tails (an extension of the HB), populated by very hot BHB stars and extreme horizontal branch (EHB) stars. Published data on the BHB stars argue that the hot BHB stars show remarkable differences in physical properties when compared to the cool BHB stars. Using high-precision photometry of stars in M 13, Ferraro et al. (1998) have found gaps in the distribution of stars along the blue tail. One of these gaps, labeled as G1, is located at $T_{\rm eff} \sim 11\,000-12\,000$ K. Grundahl et al. (1998) used the results of Strömgren *uvbyβ*-photometry finding good agreement between the theoretical prediction of stellar evolution models and the observed location of BHB stars, except for the hot BHB stars, whose *u*-magnitudes are brighter than predicted. It appears that this *u*-jump is observed for the hot BHB stars and coincides with the temperature range of the G1 gap in M 13. Similar *u*-jumps have also been found for other globular clusters (Grundahl et al. 1999). For the hot BHB with effective temperatures up to 20 000 K, the surface gravities derived from the fits of Balmer and helium line profiles appear to be lower than the predictions of stellar evolution models, while the gravities derived for the stars outside this temperature range are in good agreement with theoretical predictions (Moehler et al. 1995, 1997a,b, 2003). The stellar rotation velocity distribution of BHB stars also appears to have a discontinuity at $T_{\rm eff} \simeq 11\,500$ K (Peterson et al. 1995; Behr et al. 2000a; Recio-Blanco et al. 2004), indicating that the hotter stars show modest rotation with $v \sin i < 10$ km s^{-1}, while the cooler stars rotate more rapidly

⋆ Full Table 3 is only available in electronic form at http://www.aanda.org
⋆⋆ *Current address*: US Naval Observatory, 3450 Massachusetts Avenue NW, Washington DC 20392.
[1] Most of the known BHB stars are found in globular clusters.

Table 1. Journal of Keck+HIRES spectroscopic observations of the selected hot BHB stars from Behr (2003b).

Cluster/Star	HJD 2 450 000+	Exposure time (s)	S/N	Coverage (Å)	Seeing (arcsec)	Slit' width (arcsec)
M 13/WF2-2541	1046.7902	3×1500	44	3885–6292	0.90	0.86
M 13/WF4-3085	1052.7338	3×1200	37	3888–5356	1.10	0.86
M 13/WF4-3485	1053.7793	3×1200	34	3888–5356	0.90	0.86
M 15/B84	1053.9024	4×1400	34	3888–5356	0.80	0.86
M 15/B267	1053.9731	4×1400	26	3888–5356	0.80	0.86
M 15/B279	1053.8312	4×1400	34	3888–5356	0.90	0.86

on average. Comprehensive surveys of abundances also show that the hot BHB stars have abundance anomalies when compared to the cool BHB stars in the same cluster (Glaspey et al. 1989; Grundahl et al. 1999; Behr et al. 1999, 2000b, Behr 2003a; Fabbian et al. 2005; Pace et al. 2006).

The observed phenomena such as the low gravity, photometric jumps and gaps, abundance anomalies and slow rotation suggest that atomic diffusion could be important in the stellar atmospheres of hot BHB stars. Atomic diffusion arises from the competition between radiative acceleration and gravitational settling. This can produce a net acceleration on atoms and ions, which results in their diffusion through the atmosphere (Michaud 1970). In order for atomic diffusion to produce a vertical stratification of the abundances of particular elements, the stellar atmosphere must be hydrodynamically stable. According to Landstreet (1998), photospheric convection should be very weak at the effective temperatures of BHB stars. Theoretical atmospheric models of Hui-Bon-Hoa et al. (2000) showed that the observed photometric jumps and gaps for hot BHB stars can be explained by elemental diffusion in their atmosphere. Behr (2003b) has shown that adoption of a microturbulent velocity of 0 or 1 km s^{-1} provides the best fit to line strengths in the spectra of hot BHB stars. This fact supports the proposal that strong velocity fields are not present in the atmospheres of hot BHB stars.

While synthesizing spectral line profiles, Khalack et al. (2007) have recently found vertical abundance stratification of sulfur in the atmosphere of the field BHB star HD 135485. In this paper we also attempt to detect signatures of vertical abundance stratification of elements from line profile analyses of several other BHB stars for which we have appropriate data. Together with the data on stratification of the sulfur abundance in HD 135485, new positive results would provide a convincing argument in favour of efficient atomic diffusion in the atmospheres of hot BHB stars. In Sect. 2 we discuss the properties of the acquired spectra, while in Sect. 3 we describe details concerning the simulation routine and adopted atmospheric parameters for the program stars. The evidence for vertical stratification of some chemical species is given in Sect. 4, while the estimation of mean abundances and velocities is described in Sect. 5. A discussion follows in Sect. 6.

2. Observations

In this paper we have selected hot BHB stars from the list of objects published by Behr (2003b) and which have comparatively high signal-to-noise ratio (S/N) spectra available. Spectroscopic observations of the selected stars were undertaken in August 1998 with the Keck I telescope and the HIRES spectrograph. The journal of spectroscopic observations is shown in Table 1 where individual columns give the object identification, the heliocentric Julian Date of the observation, the exposure time, the S/N per pixel, the spectral coverage, the size of the seeing disk (FWHM) and the size of the C1 slit that provides a spectral resolution of $R = \lambda/\delta\lambda = 45\,000$. For the aforementioned stars, Behr (2003b) has found that the underfilling of the slit should not change the estimated spectral resolution by more than 4−7%.

Table 2. Parameters of stellar atmospheres for the selected hot BHB stars from Behr (2003b).

Cluster/Star	$T_{\rm eff}$ (K)	$\log g$ (dex)	ξ (km s^{-1})	$V_{\rm r}$ (km s^{-1})
M13/WF2-2541	13 000	4.0	0.0	–257.5
M13/WF4-3085	14 000	4.0	0.0	–255.7
M13/WF4-3485	13 000	4.0	0.0	–246.8
M15/B84	12 000	3.5	0.5	–108.2
M15/B267	11 000	3.5	0.0	–114.4
M15/B279	11 000	3.5	0.9	–104.4

The package of routines developed by McCarthy (1990) for the FIGARO data analysis package (Shortridge 1993) was employed to process the spectra. A comprehensive description of the data acquisition and reduction procedure is presented by Behr (2003b). This followed a standard prescription with bias subtraction, flat-fielding, order extraction, and wavelength calibration from thorium-argon comparison lamp observations. To minimize the potential distortion of narrow spectra features, cosmic ray hits were identified and removed by hand.

3. Line profile simulations

3.1. Stellar atmosphere parameters

The line profile simulations were performed with the ZEEMAN2 spectrum synthesis code (Landstreet 1988; Wade et al. 2001). The stellar atmosphere models were calculated with the PHOENIX code (Hauschildt et al. 1997) assuming LTE (Local Thermodynamic Equilibrium) and using the stellar atmosphere parameters extracted from Behr (2003b) and listed in Table 2. In calculating the stellar atmosphere models for program stars, we have used solar metallicity with the enhanced iron and depleted helium abundances derived by Behr (2003b). The depleted helium abundance has also been taken into account during line profile simulations using ZEEMAN2. We used Gaussian instrumental profiles with widths derived from the comparison arc spectra.

To simulate the spectra of BHB stars, Behr (2003b) initially adopted a microturbulent velocity $\xi = 2$ km s^{-1} and subsequently updated it during the simulation routine according to the results of his model fits. He has obtained best fit values of ξ from 0 to 0.9 km s^{-1} for the BHB stars studied here (see Table 2). Since we search for possible vertical abundance stratification, our results can be affected by microturbulence. To estimate this influence we have adopted here two different microturbulent velocities $\xi =$ 0 and 2 km s^{-1} for our simulations.

Table 3. List of iron spectral lines used for the abundance analysis.

λ, Å	$\log gf$	E_i, cm^{-1}	$\log\gamma_{\rm rad}$	Ref.	Object name					
		Fe II			WF2-2541	WF4-3085	WF2-3585	B84	B267	B279
4122.668	–3.300	20 830.58	8.49	R&U	...	x	...	x	...	...
4128.748	–3.578	20 830.58	8.61	R&U	...	x	...	...	...	x
4173.461	–2.617	20 830.58	8.61	R&U	x	x	x	x	x	...
4177.618	–3.776	73 395.93	8.61	R&U	...	x	...	x	...	x
4177.692	–3.449	20 516.96	8.61	R&U	...	x	...	x	...	x
4178.862	–2.535	20 830.58	8.49	R&U	x	x	x	x	...	x
4184.261	–1.938	90 397.87	8.35	R&U	...	x	...	...	...	...

Table 3 is presented in full in electronic form. A portion is shown here for guidance and content.

3.2. Procedure

We examined the spectrum of each star to establish a line list suitable for abundance and stratification analysis. The line identification was performed using the VALD-2 (Kupka et al. 1999; Ryabchikova et al. 1999), Pickering et al. (2001) and Raassen & Uylings[2] (1998) line databases. For all of the program stars the best represented element (with a number of readily visible line profiles) is iron. Some stars also show Ti II or P II lines. Therefore iron, titanium and phosphorus were selected for analysis of their possible vertical abundance stratification. For Fe II lines, we extracted atomic data from Raassen & Uylings (1998), while for P II lines we used VALD-2. Atomic data for Ti II lines were taken from Pickering et al. (2001).

The ZEEMAN2 code has been modified (Khalack & Wade 2006) to allow for an automatic minimization of the model parameters using the *downhill simplex method* (Press et al. 1992). The minimization routine finds the global minimum of the χ^2 function, which is specified as the measure of differences between simulated and observed line profiles. The relatively poor efficiency of the downhill simplex method, requiring a large number of function evaluations, is a well known problem. However, repeating the minimization routine several times in the vicinity of a supposed minimum in the chosen parameter space allows us to verify if the method converges to the global minimum (for more details about this minimization routine see Khalack et al. 2007).

To search for the presence of abundance stratification, we have estimated the abundance of a chemical element from an independent analysis of each selected line profile. This method operates with three free model parameters (the element's abundance, the radial velocity $V_{\rm r}$ and $v\sin i$) that are derived from each line profile using the aforementioned automatic minimization routine. To analyse the vertical abundance stratification in this method we build the scale of optical depths τ_{5000} for the list of selected line profiles. First, we calculate the line optical depth τ_ℓ in the line core for every layer of the stellar atmosphere model. Next, we suppose that each analyzed profile is formed mainly at $\tau_\ell = 1$, which corresponds to a particular layer of the stellar atmosphere with respective continuum optical depth τ_{5000}. All simulations are performed with stellar atmosphere models that contain 50 layers.

In general, we have selected for our analysis lines found to be free of predicted or inferred blends. However, if a blend is from a line of the same element that forms the main line profile, such a line was also included in our simulation. When a simulated line profile results in a radial velocity which differs significantly (more than 2 km s^{-1}) from the average $V_{\rm r}$ for the analysed star, we exclude such a line from further consideration. The difference in radial velocity may be evidence of line misidentifications or inaccurate line wavelengths. Atomic data (and sources) for the final list of iron lines selected for our study are given in Table 3.

[2] ftp://ftp.wins.uva.nl/pub/orth

4. Vertical abundance stratification

Applying the technique described in Sect. 3.2, we have attempted to determine if the iron abundance is vertically stratified in the atmospheres of the six selected BHB stars. For comparison, we have also investigated the possible vertical stratification of titanium and phosphorus for some BHB stars, where these elements are represented by a sufficient number of spectral lines.

All of the selected BHB stars are slowly rotating and have sharp absorption lines that result in only 8 to 13 spectral bins per line profile. This fact, together with the S/N and the uncertainties in the atomic data, are the main contributors to errors in the abundance inferred from a single line. This makes the detection of weak vertical abundance variations difficult.

Our abundance analysis for $\xi = 0$ km s^{-1} shows that in the atmospheres of four BHB stars (B267, B279, WF4-3085 and WF2-2541) the iron abundance generally increases towards the deeper atmospheric depths (see Figs. 1–5). It should be noted that the range of optical depths diagnosed by the iron lines is much smaller in the stars B279 and WF2-2541 than in the other two stars shown here. To estimate the stratification profile of the iron abundance we fit the data with a straight line using a least-square algorithm. We have also checked the dependence of each element's abundance with respect to the lower level excitation potential E_i for the sample of analyzed lines (see as an example Fig. 3). Slopes of the linearly approximated dependence of each element's abundance with respect to $\log E_i$ and $\log\tau_{5000}$ are given in Table 4 for the case of zero microturbulent velocity. Table 4 shows a clear correlation between the slope of the abundance versus $\log\tau_{5000}$ and $\log E_i$ for the elements considered in each star. This correlation strongly suggests that the obtained stratification is physical and not due to uncertainties in the description of the temperature profile of the stellar atmosphere.

The detected stratification of iron, obtained in some of the stars studied here, is far too large (>2 dex) to be interpreted as the result of measurement errors. Our stellar atmosphere models were calculated taking into account the enhanced iron abundance and helium depletion (Behr 2003b) and the error in estimating the iron abundances, for a given model atmosphere, is expected to be less than 0.2 dex. Meanwhile, Khan & Shulyak (2007) have shown that using atmospheric models with varying Fe abundance (from one to ten times solar) can modify the abundances inferred from observed line profiles by up to ±0.25 dex.

From the results in Table 4 we can conclude that no detectable iron stratification exists in WF4-3485 and B84. Two

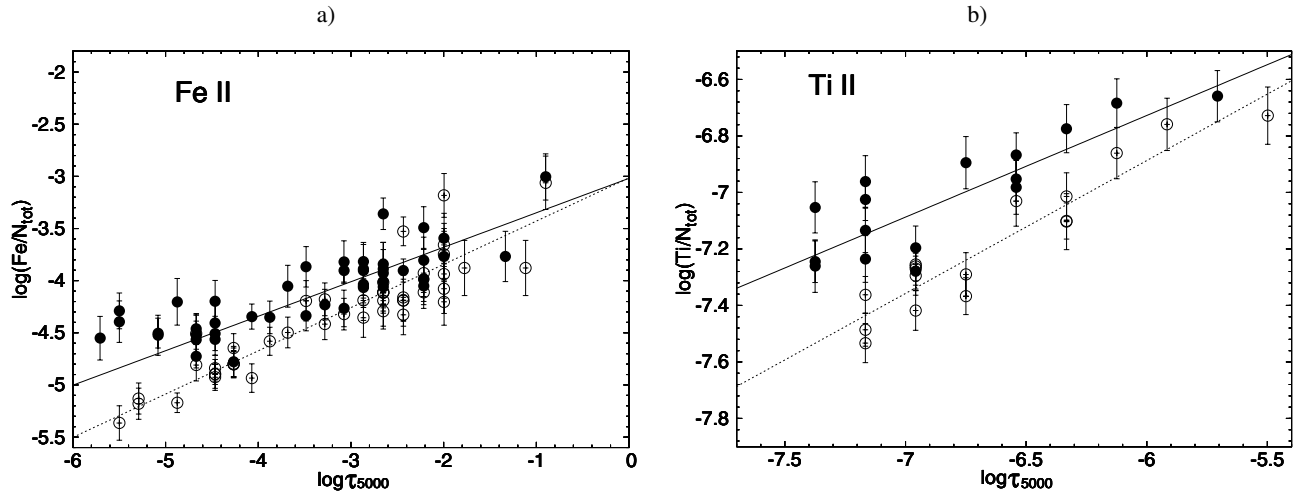

Fig. 1. Abundance estimates from the analysis of **a)** Fe II and **b)** Ti II lines as a function of line (core) formation optical depth assuming ξ = 0 km s^{-1} (filled circles) and ξ = 2 km s^{-1} (open circles) for B267. The solid and dashed lines approximate the filled and open circles respectively with straight line using the least-square algorithm.

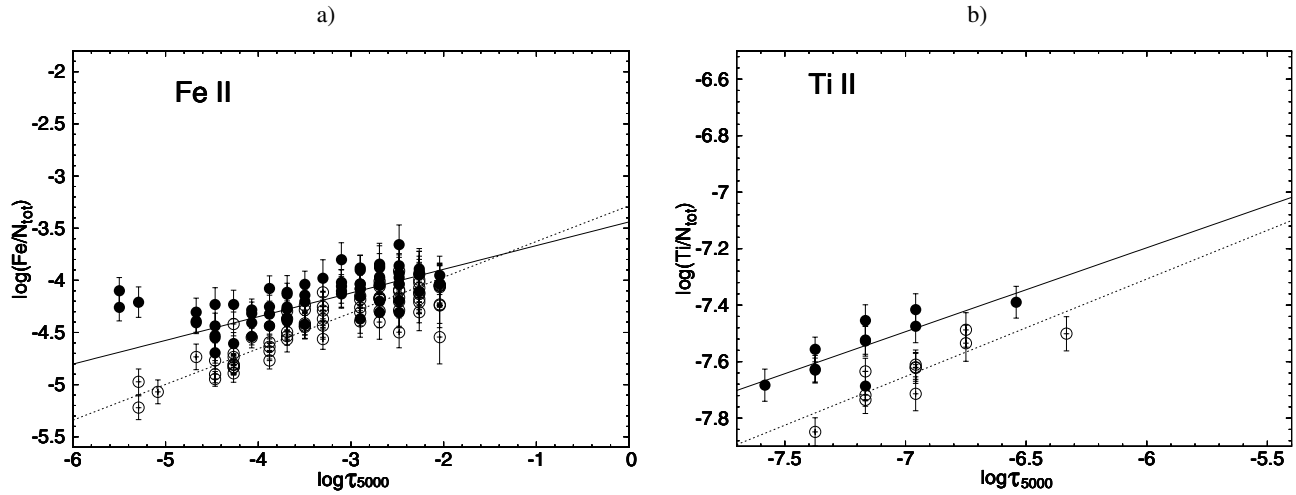

Fig. 2. The same as in Fig. 1, but for **a)** Fe II and **b)** Ti II lines extracted from the B279 spectrum.

stars (B267 and B279) show quite large slopes of iron abundance with respect to both $\log E_i$ and $\log \tau_{5000}$. The corresponding slopes for the stars WF2-2541 and WF2-3085 are smaller but still statistically significant. The least significant of these slopes is that of the abundance versus $\log E_i$ for WF2-3085 which has only approximately a 3σ value.

Another factor that must be evaluated that could mimic stratification is an error in the effective temperature of the underlying atmospheric model used. To verify the potential importance of this factor, we calculated the Fe stratification with models with an effective temperature higher and lower by 1000 K from the $T_{\rm eff}$ values listed in Table 2. We also calculated the stratification with models assuming solar He and Fe abundances to evaluate the effect of this change on the inferred stratification profiles. Our simulations show that models with higher $T_{\rm eff}$ and models with solar abundances usually slightly decrease the slope of the abundance with respect to $\log E_i$, while models with lower $T_{\rm eff}$ increase this slope for all elements. In the case of iron in WF4-3085, the model with higher $T_{\rm eff}$ and the model with solar abundances result in a negligible slope of its abundance versus $\log E_i$. Therefore, the results are not sufficient to report unambiguous detection of vertical stratification of iron in WF4-3085. The slopes for iron found for the other three stars (B267, B279 and WF-2541) are still significant in all these models, and stratification is therefore confirmed.

The two BHB stars (B84 in M 15 and WF4-3485 in M 13) which do not show any signs of stratification of their iron abundances are not different from the other stars with regards to their stellar atmosphere characteristics and rotation (see Table 2). However, these two stars possess very small titanium and phosphorus abundances as compared to the other stars studied here. Their spectra have very weak or invisible Ti II and P II lines. Their iron abundance is also close to the solar value, at least for ξ = 0 km s^{-1} (see Table 5).

We observe an upturn in the iron abundance obtained assuming ξ = 0 km s^{-1} at low optical depths for some of the stars studied (e.g. Figs. 1a, 2a, 4a, 5a). The points on the figures corresponding to the upturn feature are the strong Fe II lines and are not taken into account during the least-square fit of the data. To estimate the influence of microturbulence we have performed an abundance analysis with ξ = 2 km s^{-1}, which leads to elimination of the upturn (see, for example, Fig. 1a). Performing a set of simulations with different microturbulent velocities, we have determined the minimum value of the microturbulence ($\xi_{\rm min}$) for which the upturn disappears for each star studied. These values are reported in Table 5. As the inclusion of microturbulent

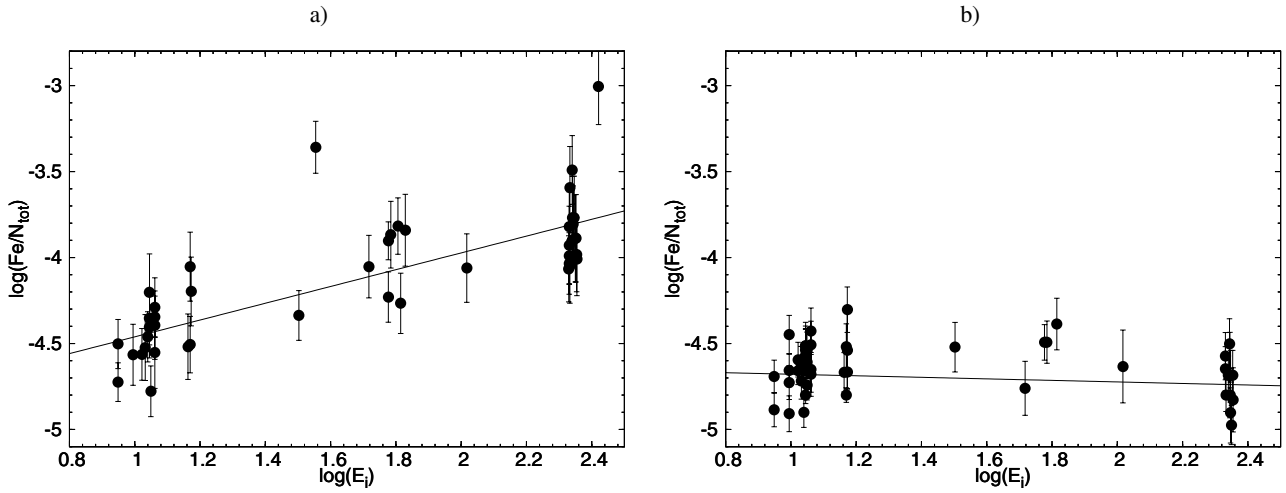

Fig. 3. Dependence of iron abundance on the lower level excitation potential of Fe II lines extracted from **a)** B267 and **b)** WF4-3485 spectra. The linear least-square fit to the data is shown by solid lines. Here the star B267 shows direct evidence of iron stratification, while WF4-3485 does not.

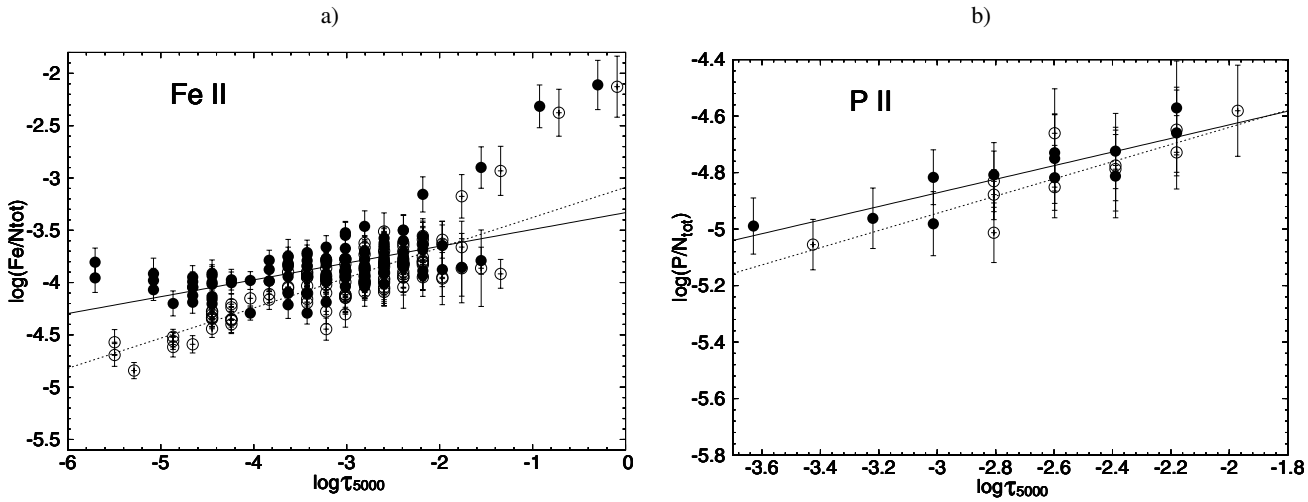

Fig. 4. The same as in Fig. 1, but for **a)** Fe II and **b)** P II lines extracted from the WF4-3085 spectrum. Here the visual strong rise in iron abundance at large optical depth manifests itself by four lines and may be real. Nevertheless, to draw the final conclusion we need more data for this range of optical depths.

Table 4. Slopes of vertical abundance stratification calculated for the linear least-square fit to the data assuming zero microturbulence.

Cluster/Star	Slopes of log (Fe/N_{tot}) vs.		n	Slopes of log (P/N_{tot}) vs.		n
	log E_i	log τ_{5000}		log E_i	log τ_{5000}	
M 13/WF2-2541	0.18 ± 0.04	0.17 ± 0.03	53	–0.67 ± 0.31	–0.14 ± 0.06	16
M 13/WF4-3085	0.10 ± 0.03	0.15 ± 0.02	117	0.54 ± 0.31	0.24 ± 0.04	12
M 13/WF4-3485	–0.06 ± 0.03	–0.02 ± 0.03	50	...	...	...
M 15/B84	0.04 ± 0.05	0.03 ± 0.04	25	...	...	...
				Slopes of log (Ti/N_{tot}) vs.		
M 15/B267	0.49 ± 0.06	0.33 ± 0.03	46	0.47 ± 0.10	0.36 ± 0.07	16
M 15/B279	0.23 ± 0.04	0.23 ± 0.02	71	0.21 ± 0.11	0.30 ± 0.08	11

velocity amplifies the iron stratification, the stratification obtained for iron in the first four stars studied with $\xi = 0$ km s^{-1} can be considered to be a lower limit to the possible stratification in these stars. A more detailed study including abundance stratification in the calculation of the synthesized spectra might shed some light on this strange behaviour, but this is outside of the scope of the present paper.

Figure 1b indicates that B267 shows a possible signature of vertical stratification of the titanium abundance. The respective slopes of Ti abundance versus log E_i and log τ_{5000} are significantly higher than zero for this star and are statistically significant (see Table 4). For B279, we can not confidently conclude that stratification exists since the slope of the abundance with respect to log E_i becomes weak when using either solar abundances or assuming a $T_{\rm eff}$ increase of 1000 K. The slope of Ti abundance with respect to log τ_{5000} also becomes weak in the model assuming a $T_{\rm eff}$ increase of 1000 K. It should be noted that the Ti lines in B279 do not sample a large portion of the atmosphere and this fact renders the detection of stratification more difficult.

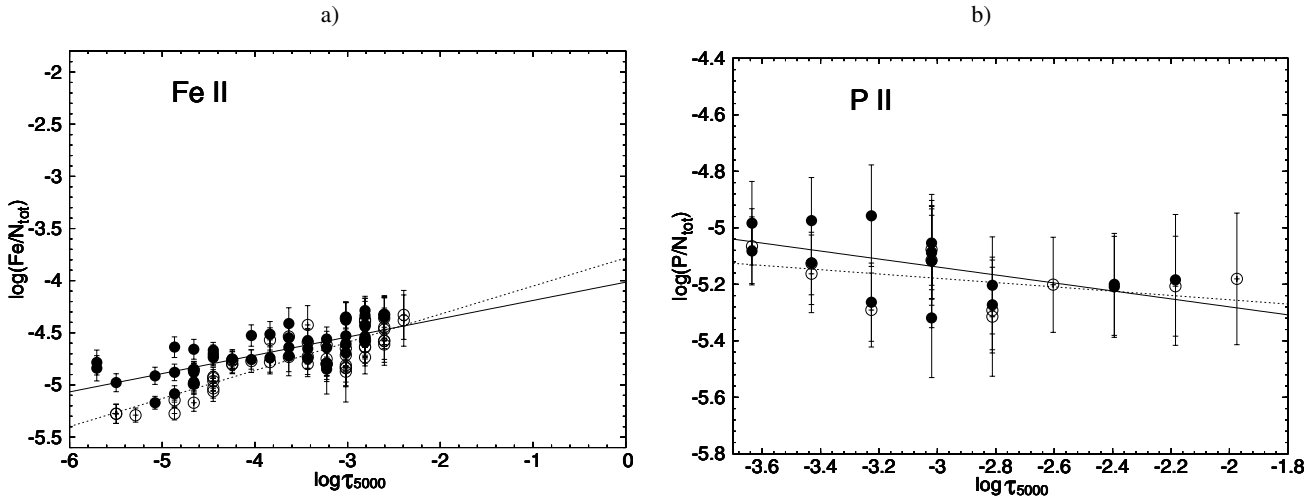

Fig. 5. The same as in Fig. 4, but for lines extracted from WF2-2541 spectrum.

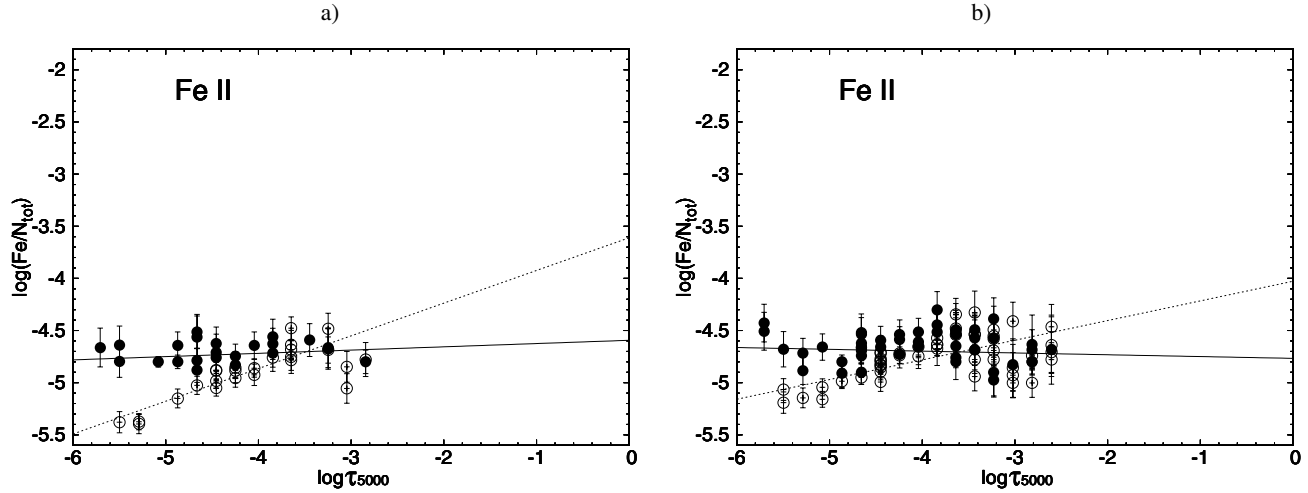

Fig. 6. The same as in Fig. 1, but for Fe II lines extracted for **a)** B84 and **b)** WF4-3485.

Table 5. Characteristics of our sample of hot BHB stars obtained from spectral simulations.

Cluster/Star	$v \sin i$	V_r	ξ_{min}	[Fe/H]			[P/H]		
	km s^{-1}	km s^{-1}	km s^{-1}	ξ = 0 km s^{-1}	ξ = 2 km s^{-1}	n	ξ = 0 km s^{-1}	ξ = 2 km s^{-1}	n
M 13/WF2-2541	2.4 ± 0.5	–257.3 ± 0.5	0.0+0.3	–0.12 ± 0.20	–0.19 ± 0.26	53	+1.51 ± 0.11	+1.46 ± 0.10	16
M 13/WF4-3085	3.4 ± 0.8	–255.4 ± 0.5	0.5 ± 0.3	+0.72 ± 0.29	+0.59 ± 0.37	117	+1.84 ± 0.13	+1.84 ± 0.15	12
M 13/WF4-3485	3.0 ± 0.9	–246.9 ± 0.9	1.5 ± 0.3	–0.04 ± 0.50	–0.17 ± 0.27	50	...	...	...
M 15/B84	4.0 ± 1.3	–108.3 ± 0.4	0.0+0.3	–0.14 ± 0.10	–0.35 ± 0.24	25	...	...	...
							[Ti/H]		
M 15/B267	6.2 ± 1.2	–114.7 ± 0.7	0.5 ± 0.3	+0.45 ± 0.37	+0.21 ± 0.51	46	+0.09 ± 0.20	–0.08 ± 0.24	16
M 15/B279	4.7 ± 1.6	–104.5 ± 0.6	1.0 ± 0.3	+0.42 ± 0.34	+0.20 ± 0.40	71	–0.44 ± 0.10	–0.54 ± 0.11	11

It is clear that phosphorous shows no clear signs of stratification in WF2-2541. For WF4-3085 we cannot make firm conclusions concerning phosphorous stratification since its abundance variation in the range of optical depths under consideration is only approximately 0.4 dex. Also, the slope of its abundance with respect to $\log E_i$ is not statistically significant.

5. Mean abundances and velocities

The mean photospheric abundances derived for the selected BHB stars from an analysis of the available iron, titanium and phosphorus lines are reported in Table 5. For each chemical element, three columns are shown containing the mean abundance for simulations with microturbulent velocity ξ = 0 and 2 km s^{-1} respectively, and the number of analyzed line profiles. The reported uncertainties are equal to the standard deviation calculated from the results of individual line simulations for all lines considered.

The derived heliocentric radial and projected rotation velocities as well as microturbulent velocities (see Table 5) are generally in agreement with the data provided by Behr (2003b) for these stars. Some inconsistencies are found between $v \sin i$ values obtained for WF2-2541 ($v \sin i = 0.0^{+4.07}_{-0.0}$ km s^{-1}) and B279 ($v \sin i = 5.92^{+1.6}_{-1.69}$ km s^{-1}), but they are within the respective

error bars given by Behr (2003b). The precision of our velocity estimates appears to be comparatively higher because of a more stringent selection of analysed line profiles. Our measurements of the average abundance of iron, titanium and phosphorus also agree with the corresponding values published by Behr (2003b), taking into account the error bars and the value of the applied microturbulent velocity. Small differences between our results and abundances from the aforementioned paper are not surprising. Our average abundance is calculated with the individual abundances obtained from each line, while Behr (2003b) fitted the whole spectrum of each element to obtain its abundance.

6. Discussion

In this paper we continue our attempts to detect vertical abundance stratification in the atmospheres of BHB stars. After the report by Bonifacio et al. (1995) of the vertical stratification of helium in the atmosphere of Feige 86, it became clear that the abundances of other chemical species may also be stratified. We devoted special interest to iron because hot BHB stars usually have an enhanced iron abundance (e.g. Behr 2003b), suggesting that this element may be strongly affected by diffusion. Analysing the spectra of another hot BHB star HD 135485 (Khalack et al. 2007) we did not find direct evidence of iron stratification, but revealed strong signatures of sulfur depletion in the deeper atmospheric layers. However, HD 135485 is different from the other BHB stars in that its spectrum shows evidence of helium enrichment (in comparison with the solar abundance), while in the atmospheres of the other BHB stars helium is depleted.

Therefore, we directed our attention to BHB stars where the iron abundance is near the solar abundance or enhanced, and helium is depleted. The results obtained argue that at least three stars (B267 and B279 in M 15 and WF2-2541 in M 13) show clear signatures of vertical stratification of their iron abundance, while for WF4-3085 the results are suggestive, but not conclusive. The other two stars studied here (B84 in M 15 and WF4-3485 in M 13) do not show stratification of iron and their averaged iron abundance is close to solar (but is enhanced in comparison with its cluster value). B267 shows also a signature of vertical stratification of titanium (see Fig. 1b).

Since our simulations show that the turnup feature observed in the iron stratification profile is strongly dependent on microturbulent velocity, the value of the abundance at low optical depths is uncertain. Of course, if the theoretical framework supposes that these abundance gradients are due to atomic diffusion, microturbulence should be weak since a stable atmosphere is needed for diffusion to be dominant. It should be noted that for corresponding optical depths the abundance profile of iron is similar in the three BHB stars that exhibit stratification. The reason that the other two stars in our study do not show clear signs of iron stratification (B84 and WF4-3485) might be related to evolutionary effects or the presence of other competing hydrodynamical processes. The absence of Ti II and P II lines in their spectra might be evidence of this.

In conclusion, the results shown here add to the mounting evidence of the existence of vertical abundance stratification, and hence atomic diffusion, in the atmospheres of BHB stars.

Acknowledgements. This research was partially funded by the Natural Sciences and Engineering Research Council of Canada (NSERC). We thank the Réseau québécois de calcul de haute performance (RQCHP) for computing resources. G.A.W. acknowledges support from the Academic Research Programme (ARP) of the Department of National Defence (Canada). B.B.B. thanks all the dedicated people involved in the construction and operation of the Keck telescopes and HIRES spectrograph. He is also grateful to Judy Cohen, Jim McCarthy, George Djorgovski, and Pat Côté for their contributions of Keck observing time. We are grateful to Dr. T. Ryabchikova and Dr. L. Mashonkina for helpful discussions and suggestions.

References

Behr, B. B. 2003a, ApJS, 149, 67
Behr, B. B. 2003b, ApJS, 149, 101
Behr, B. B., Cohen, J. G., McCarthy, J. K., & Djorgovski, S. G. 1999, ApJ, 517, L135
Behr, B. B., Djorgovski, S. G., Cohen, J. G., et al. 2000a, ApJ, 528, 849
Behr, B. B., Cohen, J. G., & McCarthy, J. K. 2000b, ApJ, 531, L37
Bonifacio, P., Castelli, F., & Hack, M. 1995, A&AS, 110, 441
Fabbian, D., Recio-Blanco, A., Gratton, R. G., & Piotto, G. 2005, A&A, 434, 235
Ferraro, F. R., Paltrinieri, B., Fusi Pecci, F., et al. 1998, ApJ, 500, 311
Glaspey, J. W., Michaud, G., Moffat, A. F. J., & Demers, S. 1989, ApJ, 339, 926
Grundahl, F., Vandenberg, D. A., & Andersen, M. I. 1998, ApJ, 500, L179
Grundahl, F., Catelan, M., Landsman, W. B., et al. 1999, ApJ, 524, 242
Hauschildt, P. H., Baron, E., & Allard, F. 1997, ApJ, 483, 390
Hui-Bon-Hoa, A., LeBlanc, F., & Hauschildt, P. H. 2000, ApJ, 535, L43
Khalack, V., & Wade, G. 2006, A&A, 450, 1157
Khalack, V., LeBlanc, F., Bohlender, D., et al. 2007, A&A, 466, 667
Khan, S. A., & Shulyak, D. V. 2007, A&A, 469, 1083
Kupka, F., Piskunov, N. E., Ryabchikova, T. A., et al. 1999, A&AS, 138, 119
Landstreet, J. D. 1988, ApJ, 326, 967
Landstreet, J. D. 1998, Contrib. Astron. Obs. Scalnaté Pleso, 27, 350
McCarthy, J. K. 1990, in Proc. 2nd ESO/ST-ECF Data Analysis Workshop (Garching: ESO), 119
Michaud, G. 1970, ApJ, 160, 641
Moehler, S. 2004, Proc. IAU Symp. 224, ed. J. Zverko, W. W. Weiss, J. Ziznovsky, & S. J. Adelman, 119
Moehler, S., & Sweigart, A. V. 2006, A&A, 455, 943
Moehler, S., Heber, U., & DeBoer, K. S. 1995, A&A, 294, 65
Moehler, S., Heber, U., & Durrell, P. R. 1997a, A&A, 317, L83
Moehler, S., Heber, U., & Rupprecht, G. 1997b, A&A, 319, 109
Moehler, S., Landsman, W. B., Sweigart, A. V., & Grundal, F. 2003, A&A, 405, 135
Pace, G., Recio-Blanco, A., Piotto, G., & Momany, Y. 2006, A&A, 452, 493
Peterson, R. C., Rood, R. T., & Crocker, D. A. 1995, ApJ, 453, 214
Pickering, J. C., Thorne, A. P., & Perez, R. 2001, ApJS, 132, 403
Press, W. H., Teukolsky, S. A., Vetterling, W. T., & Flannery, B. P. 1992, Numerical recipes in C: the art of scientific computing, 2nd Ed. (Cambridge University Press), 995
Raassen, A. J. J., & Uylings, P. H. M. 1998, A&A, 340, 300
Recio-Blanco, A., Piotto, G., Aparicio, A., & Renzini, A. 2004, A&A, 417, 597
Ryabchikova, T. A., Piskunov, N. E., Stempels, H. C., Kupka, F., & Weiss, W. W. 1999, in Proc. of the 6th International Colloquium om Atomic Spectra and Oscillator Strengths, Victoria BC, Phys. Scr. T83, 162
Sandage, A. R., & Wallerstein, G. 1960, ApJ, 131, 598
Shortridge, K. 1993, The Figaro 2.4 Manual
Wade, G. A., Bagnulo, S., Kochukhov, O., et al. 2001, A&A, 374, 265

Online Material

Table 3. List of iron spectral lines used for the abundance analysis.

λ, Å	$\log gf$	E_i, cm^{-1}	$\log \gamma_{\rm rad}$	Ref.	Object name					
		Fe II			WF2-2541	WF4-3085	WF2-3585	B84	B267	B279
3903.756	−1.555	60 807.23	8.99	R&U		x				
3906.035	−1.704	44 929.55	8.72	R&U		x	x			x
3918.528	−2.485	47 674.72	8.55	R&U		x				x
3920.635	−1.335	60 625.45	9.01	R&U		x	x		x	x
3924.838	−1.103	78 137.36	8.93	R&U		x				
3938.970	−1.932	47 674.72	8.61	R&U		x				x
3945.210	−4.440	13 673.18	8.46	R&U						x
4002.083	−4.481	22 409.85	8.53	R&U		x				
4002.543	−2.072	48 039.09	8.68	R&U		x				
4016.367	−1.420	75 600.93	9.01	R&U		x				
4024.547	−2.439	36 252.92	8.49	R&U		x	x		x	x
4032.945	−1.920	79 331.50	9.18	R&U		x				x
4044.012	−2.671	44 929.55	8.70	R&U						x
4048.832	−2.381	44 917.07	8.73	R&U		x			x	x
4122.668	−3.300	20 830.58	8.49	R&U		x		x		
4128.748	−3.578	20 830.58	8.61	R&U		x				x
4173.461	−2.617	20 830.58	8.61	R&U	x	x	x	x	x	
4177.618	−3.776	73 395.93	8.61	R&U		x		x		x
4177.692	−3.449	20 516.96	8.61	R&U		x		x		x
4178.862	−2.535	20 830.58	8.49	R&U	x	x	x	x		x
4184.261	−1.938	90 397.87	8.35	R&U		x				
4217.899	−0.976	90 777.81	8.51	VALD					x	
4233.172	−1.947	20 830.58	8.61	R&U		x	x		x	
4258.154	−3.478	21 812.06	8.48	R&U		x				x
4258.340	−4.301	21 308.04	8.61	R&U						x
4263.869	−1.696	62 049.03	8.95	R&U		x				
4273.326	−3.303	21 812.06	8.62	R&U	x	x	x			x
4286.280	−1.730	62 171.61	8.96	R&U		x				
4296.572	−2.933	21 812.06	8.49	R&U		x	x	x		x
4303.176	−2.511	21 812.06	8.61	R&U	x	x	x		x	
4314.979	−3.193	38 164.19	8.49	R&U					x	x
4351.769	−2.216	21 812.06	8.61	R&U	x		x			
4357.584	−2.010	49 100.98	8.64	R&U					x	
4361.205	−2.827	62 125.60	8.94	R&U		x				
4361.247	−2.264	49 506.93	8.70	R&U		x				
4369.411	−3.584	22 409.85	8.48	R&U						x
4384.319	−3.684	21 430.36	8.48	R&U		x				x
4385.381	−2.581	22 409.85	8.62	R&U	x	x	x			
4416.830	−2.602	22 409.85	8.61	R&U	x	x	x		x	x
4451.551	−1.907	49 506.93	8.74	R&U		x	x		x	x
4455.266	−2.000	50 212.83	8.58	R&U						x
4461.694	−4.002	63 272.98	9.02	R&U	x	x				x
4461.706	−2.065	50 212.83	8.62	R&U	x	x				x
4472.929	−3.531	22 939.36	8.48	R&U		x	x			x
4489.183	−2.971	22 810.36	8.49	R&U	x		x			x
4491.405	−2.755	23 031.30	8.48	R&U		x	x	x	x	x
4493.529	−1.555	63 876.32	9.00	R&U		x				

Table 3. continued.

λ, Å	$\log gf$	E_i, cm^{-1}	$\log \gamma_{\rm rad}$	Ref.	Object name					
		Fe II			WF2-2541	WF4-3085	WF2-3585	B84	B267	B279
4508.214	−2.589	63 948.79	9.01	R&U	x	x	x			x
4508.288	−2.349	23 031.30	8.62	R&U	x	x	x			x
4515.339	−2.540	22 939.36	8.49	R&U		x	x	x	x	
4520.224	−2.617	22 637.21	8.49	R&U	x	x				x
4522.634	−2.169	22 939.36	8.61	R&U	x	x	x	x	x	
4534.168	−3.364	23 031.30	8.49	R&U	x	x				
4541.524	−2.973	23 031.30	8.61	R&U		x	x	x		x
4549.192	−1.767	47 674.72	8.70	R&U	x	x	x		x	
4549.474	−2.016	22 810.36	8.61	R&U	x	x	x			
4555.893	−2.421	22 810.36	8.49	R&U	x	x	x	x	x	
4576.340	−2.976	22 939.36	8.61	R&U			x			x
4579.527	−2.343	50 212.83	8.64	R&U					x	x
4582.835	−3.224	22 939.36	8.49	R&U	x	x	x	x	x	x
4583.837	−1.867	22 637.21	8.61	R&U	x	x	x	x	x	
4596.015	−1.956	50 212.83	8.74	R&U	x	x				x
4598.494	−1.512	62 945.04	9.00	R&U		x				
4620.521	−3.315	22 810.36	8.61	R&U	x	x		x		x
4628.786	−1.724	63 272.98	9.01	R&U		x				
4629.339	−2.478	22 637.21	8.48	R&U	x	x	x			x
4635.316	−1.578	48 039.09	8.73	R&U	x	x	x	x	x	x
4656.981	−3.643	23 317.63	8.61	R&U		x				
4666.758	−3.368	22 810.36	8.48	R&U		x				
4731.453	−3.127	23 317.63	8.61	R&U		x	x	x	x	x
4798.673	−1.862	83 136.49	8.95	R&U			x			
4826.683	−0.512	82 978.68	8.95	R&U		x				
4913.181	−1.238	82 978.68	8.96	R&U		x			x	x
4913.292	0.019	82 978.68	8.95	R&U		x			x	x
4923.927	−1.504	23 317.63	8.49	R&U	x	x	x	x	x	x
4948.096	−0.239	83 136.49	8.99	R&U		x				
4948.793	−0.043	83 459.67	9.01	R&U		x				
4951.584	0.198	83 136.49	8.96	R&U		x	x			
4958.822	−0.693	83 713.54	8.95	R&U		x				
4977.035	−0.041	83 558.54	9.00	R&U	x	x				
4977.923	−0.606	83 308.19	9.01	R&U		x				
4984.488	0.074	83 308.19	9.01	R&U		x				
4990.509	0.193	83 308.19	8.99	R&U		x				
5001.864	0.010	31 302.42	7.97	R&U		x	x	x	x	x
5001.959	0.916	82 978.68	8.93	R&U	x	x	x	x	x	x
5004.195	0.504	82 853.66	8.93	R&U	x	x			x	x
5006.841	−0.260	83 713.54	8.93	R&U		x				
5007.447	−0.435	83 726.36	8.94	R&U		x				
5007.739	−0.273	82 978.68	9.03	R&U		x				
5018.440	−1.345	23 317.63	8.49	R&U	x	x	x	x	x	x
5021.594	−0.189	82 978.68	9.05	R&U		x				
5022.420	−0.066	83 459.67	9.01	R&U		x				
5022.792	−0.077	82 978.68	9.10	R&U	x	x				x
5026.806	−0.427	83 136.49	9.03	R&U		x				

Table 3. continued.

λ, Å	$\log gf$	E_i, cm^{-1}	$\log \gamma_{\rm rad}$	Ref.	Object name					
		Fe II			WF2-2541	WF4-3085	WF2-3585	B84	B267	B279
5029.097	−0.615	83 558.54	9.07	R&U		x				
5030.630	0.433	82 978.68	9.02	R&U	x	x			x	x
5032.712	0.107	83 812.32	8.99	R&U	x	x				x
5034.003	−0.793	83 558.54	9.02	R&U		x				
5035.708	0.639	82 978.68	8.94	R&U	x	x	x	x	x	x
5045.114	0.005	83 136.49	9.05	R&U		x			x	
5047.641	−0.216	83 136.49	9.04	R&U		x			x	
5061.718	0.290	83 136.49	9.06	R&U						x
5067.893	−0.063	83 308.19	9.06	R&U		x				
5070.899	0.275	83 136.49	9.02	R&U	x	x				x
5075.764	0.168	84 326.91	8.94	R&U	x	x				x
5082.230	−0.121	83 990.06	9.00	R&U		x			x	
5089.214	0.025	83 308.19	9.05	R&U						x
5097.271	0.315	83 713.54	8.94	R&U	x	x				x
5100.607	0.234	83 726.36	8.95	R&U	x	x	x		x	x
5100.727	0.724	83 726.36	8.94	R&U	x	x	x		x	x
5106.097	−0.961	83 812.32	9.00	R&U		x				
5106.109	−0.234	83 308.19	9.06	R&U		x				
5107.547	−0.609	83 812.32	9.17	R&U		x				
5117.034	−0.033	84 131.56	9.01	R&U		x	x			
5123.188	−2.457	62 125.60	8.49	R&U		x				
5123.188	−2.286	84 131.56	8.99	R&U		x				
5132.669	−4.094	22 637.21	8.54	R&U		x				
5143.880	−0.223	84 266.56	9.00	R&U		x				
5149.465	0.544	84 266.56	8.92	R&U	x	x				
5166.582	−0.059	84 326.91	8.98	R&U						x
5169.033	−1.250	23 317.63	8.48	R&U	x	x	x	x	x	x
5180.314	−0.103	83 812.32	9.00	R&U		x				x
5194.892	−0.103	84 424.37	8.99	R&U		x				
5197.568	−2.105	83 865.63	9.05	VALD	x	x	x	x	x	
5197.577	−2.348	26 055.42	8.48	R&U	x	x	x	x	x	
5199.122	0.107	83 713.54	9.02	R&U	x	x				
5213.960	−0.264	84 527.78	9.01	R&U		x				
5214.057	−0.633	83 713.54	9.04	R&U		x				
5215.844	−0.153	83 726.36	9.22	R&U					x	
5216.854	0.480	84 710.68	8.96	R&U		x	x		x	x
5216.863	0.659	84 527.78	8.93	R&U		x	x		x	x
5218.842	−0.181	83 726.36	9.10	R&U		x				
5223.260	−0.190	83 812.32	9.04	R&U					x	
5223.290	−0.914	84 266.56	9.09	R&U					x	
5223.800	−0.532	83 713.54	9.01	R&U		x				
5224.411	−0.450	83 990.06	9.09	R&U		x				
5227.323	0.191	84 844.83	8.93	R&U			x			
5227.481	0.834	84 296.83	8.91	R&U			x			
5232.787	−0.115	83 726.36	8.93	R&U		x				
5234.615	−2.385	84 266.56	8.98	R&U		x	x	x	x	x
5234.625	−2.279	25 981.63	8.49	R&U		x	x	x	x	x
5237.951	0.101	84 266.56	9.11	R&U		x	x			

Table 3. continued.

λ, Å	$\log gf$	E_i, cm^{-1}	$\log \gamma_{\rm rad}$	Ref.	Object name					
		Fe II			WF2-2541	WF4-3085	WF2-3585	B84	B267	B279
5247.952	0.550	84 938.18	8.95	R&U		x	x		x	x
5251.211	−0.638	84 326.91	8.99	R&U		x				
5251.233	0.442	84 844.83	9.00	R&U		x				
5254.929	−3.336	26 055.42	8.49	R&U			x			
5260.259	1.069	84 035.01	8.91	R&U			x	x		x
5262.317	−0.370	85 048.60	9.08	R&U		x				
5264.812	−3.132	26 055.42	8.61	R&U		x	x			x
5272.397	−2.009	48 039.09	8.70	R&U		x				x
5276.002	−2.213	25 805.33	8.49	R&U		x	x	x	x	x
5291.667	0.556	84 527.78	9.00	R&U	x	x				x
5306.180	0.104	84 870.86	9.06	R&U					x	
5316.225	0.340	84 035.14	8.92	R&U						x
5316.615	−2.014	25 428.78	8.48	R&U	x					x
5316.784	−2.783	25 981.63	8.61	R&U	x					x
5325.553	−3.324	25 981.63	8.49	R&U		x	x		x	x
5339.585	0.540	84 296.83	8.91	R&U	x	x	x			
5362.869	−2.616	25 805.33	8.61	R&U	x					
5362.967	−0.137	84 685.20	8.90	R&U	x					
5427.826	−1.580	54 232.19	8.54	R&U	x					
5429.988	0.438	85 462.86	8.93	R&U	x					
5465.931	0.352	85 679.70	8.91	R&U	x					
5492.079	0.089	85 679.70	8.98	R&U	x					
5506.195	0.849	84 863.35	8.89	R&U	x					
5507.072	−0.082	84 870.86	8.98	R&U	x					
5510.779	−0.092	85 184.73	8.92	R&U	x					
5544.763	0.129	84 863.35	9.21	R&U	x					
5645.392	0.176	85 184.73	9.21	R&U	x					
		Ti II								
3900.539	−0.200	9118.28	8.36	Pic.						x
3913.461	−0.420	8997.78	8.37	Pic.					x	x
4053.821	−1.130	15 265.69	8.38	Pic.					x	
4163.644	−0.130	20 891.78	8.37	Pic.					x	x
4290.215	−0.850	9395.79	8.46	Pic.					x	x
4294.094	−0.930	8744.34	8.22	Pic.					x	x
4300.042	−0.440	9518.14	8.47	Pic.					x	x
4301.922	−1.150	9363.73	8.47	Pic.					x	
4395.031	−0.540	8744.34	8.21	Pic.					x	x
4399.765	−1.190	9975.99	8.46	Pic.					x	
4443.801	−0.720	8710.56	8.20	Pic.					x	x
4468.507	−0.600	9122.14	8.21	VALD					x	
4501.270	−0.684	8997.78	8.20	VALD					x	x
4563.757	−0.690	9851.00	8.22	Pic.					x	x
4571.971	−0.230	12 677.10	8.37	Pic.						x
4805.085	−0.960	16 623.11	8.26	VALD					x	
4911.195	−0.610	25 192.96	8.30	Pic.					x	
5188.687	−1.050	12 758.26	8.22	Pic.					x	

Table 3. continued.

λ, Å	$\log gf$	E_i, cm^{-1}	$\log \gamma_{\rm rad}$	Ref.	Object name					
		P II			WF2-2541	WF4-3085	WF2-3585	B84	B267	B279
4178.463	−0.409	77 671.28		VALD	x	x				
4420.712	−0.478	88 893.22		VALD	x	x				
4463.027	0.026	105 553.90		VALD		x				
4468.000	−0.208	105 223.22		VALD		x				
4475.270	0.301	105 553.90		VALD	x	x				
4499.230	0.377	107 922.93		VALD	x	x				
4530.823	−0.020	105 303.87		VALD	x	x				
4588.032	0.575	103 343.94		VALD	x	x				
4589.846	0.500	103 166.50		VALD		x				
4602.069	0.799	103 667.86		VALD		x				
4658.309	−0.412	103 665.56		VALD		x				
4943.497	0.083	103 665.56		VALD		x				
5253.479	0.291	88 893.22		VALD	x					
5296.077	−0.134	87 124.60		VALD	x					
5316.055	−0.341	86 743.96		VALD	x					
5344.729	−0.329	86 597.55		VALD	x					
5425.880	0.241	87 124.11		VALD	x					
5499.697	−0.495	87 124.11		VALD	x					
6024.178	0.137	86 745.03		VALD	x					
6034.039	−0.209	86 599.85		VALD	x					
6043.084	0.384	87 124.11		VALD	x					
6165.598	−0.469	87 124.11		VALD	x					

R&U 1998A&A...340..300R Raassen & Uylings
VALD 1999POBeo..65..223K Kupka & Ryabchikova
Pic. 2001ApJS...132..403 Pickering, Thorne & Perez
NIST 2002nla.work...80R Reader et al.